Assessing the performance of solar thermal driven membrane distillation for seawater desalination by computer simulation

Revised Manuscript Submitted to

Journal of Membrane Science

July 2017

Hung C. Duong[1], Lei Xia[2], Zhenjun Ma[2], Paul Cooper[2], Wendell Ela[3], Long D. Nghiem[1,*]

[1] Strategic Water Infrastructure Laboratory, School of Civil, Mining and Environmental Engineering, University of Wollongong, Wollongong, NSW 2522, Australia

[2] Sustainable Buildings Research Centre, University of Wollongong, NSW 2522, Australia

[3] School of Engineering & Information Technology, Murdoch University, Murdoch, WA 6150, Australia

* Corresponding author: Long Duc Nghiem, Email longn@uow.edu.au; Tel: +61 2 4221 4590

Abstract: A computer model was developed to simulate the performance of an integrated solar thermal driven direct contact membrane distillation (DCMD) system for seawater desalination using recorded weather data. The results highlight the importance of simulating the DCMD process together with the energy source. Indeed, when considered in isolation from the thermal energy source, increasing water cross flow velocities in the feed and distillate channels results in an increase in water flux and thermal efficiency of the DCMD module. By contrast, when coupling the DCMD module with the solar thermal collector, increasing water cross flow velocities reduces both the process water flux and thermal efficiency. This is because of the limited supply of solar thermal at any given time, and hence the feed temperature decreases when cross flow velocities increase. Thus, any benefits in the reduction of temperature polarisation due to increasing cross flow velocities are overwhelmed by the effects of feed temperature decrease on water flux and thermal efficiency. Results from our simulation also demonstrate the viability of the solar thermal driven DCMD process for small-scale seawater desalination applications. Distillate production is dependent on the availability of solar radiation during the day; nevertheless, a small system with a 7.2 m^2 spiral-wound DCMD module and a 22.6 m^2 flat plate solar thermal collector can produce over 140 kg of distillate each day under real weather conditions. This is equivalent to a daily distillate production rate of 19.7 kg per m^2 of membrane or 6.3 kg per m^2 of solar thermal collector.

Keywords: *membrane distillation (MD); seawater desalination; solar thermal energy; simulation; process optimisation.*

1. Introduction

Membrane distillation (MD) has significant potential for small-scale solar thermal seawater desalination in remote coastal areas. In the MD process, a microporous hydrophobic membrane is used to facilitate the transport of water vapour while retaining liquid water and hence all non-volatile substances and dissolved salts; therefore, ultrapure water can be obtained from seawater MD desalination [1, 2]. Unlike pressure-driven membrane desalination processes such as reverse osmosis (RO), MD utilises a vapour pressure gradient induced by a temperature difference across the membrane as the driving force for water transfer. Thus, water flux in MD is not affected by the feed water osmotic pressure [3, 4].

MD is arguably the most suitable platform for small-scale and off-the-grid seawater desalination applications [5-9]. MD is less susceptible to membrane fouling than RO given the absence of a high hydraulic pressure and the discontinuity of the liquid phase across the membrane. As a result, MD can be operated without feed water pre-treatment, making it an ideal process for small and stand-alone seawater desalination applications. Furthermore, MD systems can be made from inexpensive and noncorrosive plastic materials to reduce process investment and operational costs. Finally, MD can be operated at low feed temperature [10-12]; thus, low-grade heat sources such as solar thermal energy can be utilised to meet MD energy demands.

MD can be applied in various configurations including direct contact membrane distillation (DCMD), air gap membrane distillation (AGMD), permeate gap membrane distillation (PGMD), vacuum membrane distillation (VMD), and sweeping gas membrane distillation (SGMD). Amongst these configurations, DCMD has the simplest arrangement and thus is probably best suited for small-scale seawater desalination applications [13, 14]. In DCMD, the hot feed and the cold distillate are in direct contact with the membrane, allowing for efficient heat and mass transfer to and from the feed and distillate membrane surfaces, and thus facilitating high water flux [14, 15]. However, the direct contact configuration also facilitates the heat conduction through the membrane, thus rendering DCMD less thermally efficient than other configurations.

Numerous experimental studies have been conducted to investigate the feasibility of DCMD using low-grade heat sources such as waste heat and solar thermal energy for desalination applications. Dow et al. [14] reported a sustainable operation of a pilot DCMD system over 3 months using waste heat from a thermal power station. They obtained an average water flux of 3 kg/(m^2·h) and thermal efficiency of 0.42 [14]. The low thermal efficiency obtained by Dow et al. [14] was deemed acceptable given the freely available waste heat from the power plant. Suarez et al. [16] examined a lab-scale desalination process using DCMD with low-temperature heat

extracted from a salt-gradient solar pond. Their results revealed a limited thermal efficiency, with only about 35% of the heat extracted from the solar pond was utilised for the water transfer across the membrane [16]. In another study, Shim et al. [17] evaluated a DCMD system coupled with a solar thermal collector for seawater desalination application. The solar thermal collector could provide more than 77% heating energy of the DCMD process. However, because of the low process thermal efficiency, a large area of solar thermal collector (i.e. 4.7 m^2) was required to power 0.06 m^2 DCMD membrane module [17]. Solar thermal collectors have also been utilised to power AGMD and PGMD systems for small-scale seawater desalination application [18-20].

Computer-aided simulations can play an important role in optimising module design and process operation for a solar thermal driven MD system. Simulations of complex processes during MD operation including heat and mass transfer, temperature and concentration polarisation effects, and thermal efficiency have been reported in the literature [21-25]. Computer software packages such as MATLAB, ANSYS Fluent, Aspen Custom Modeller, COMSOL Multiphysics, and Microsoft Excel have been successfully employed to perform MD simulations [21, 23, 24, 26-28]. However, in contrast to the many previous simulation studies on MD membrane module and system performance, very few works have attempted to simulate the integrated solar thermal driven MD process [29]. Unlike previous studies with a constant supply of energy, solar thermal is only available during the day and there is a significant temporal variation in the amount of thermal energy generated per square meter of collector [29, 30].

This study reported a comprehensive simulation of an integrated solar thermal driven DCMD system for small-scale seawater desalination application. First, important performance parameters including water flux, temperature polarisation effect, and thermal efficiency along the DCMD module channels under two flow modes and various operating conditions were simulated and examined. Subsequently, a solar thermal driven DCMD process, in which a solar thermal collector was coupled with the DCMD module, was simulated to demonstrate the intermittent performance of the process. The influences of operating conditions, most importantly the water cross flow velocities, on process water flux and thermal efficiency were elucidated to optimise the solar thermal seawater DCMD process. Thermal efficiency and distillate production rate of the process were analysed to elucidate the feasibility of DCMD for solar thermal driven seawater desalination. The TRNSYS, which is a transient system simulation tool [31], was used to simulate the availability of solar thermal for the MD process.

2. Theories

In MD, the transfer of mass and heat through the membrane occurs simultaneously. Water (mass) transfer is driven by the difference in partial water vapour pressure across the membrane. At the same time, heat is transferred via conduction and in the form of latent heat.

The mass transfer of water is described as:

$$J = C_m(P_{m.f} - P_{m.d}) \quad (1)$$

where J is water flux (kg/(m^2·h)), C_m is the membrane mass transfer coefficient (kg/(m^2·h·Pa)), and $P_{m.f}$ and $P_{m.d}$ are the water vapour pressure (Pa) at the feed and distillate membrane surfaces, respectively. The water vapour pressure at the membrane surfaces can be calculated as [2, 13]:

$$P = x_{water}(1-0.5x_{salt}-10x_{salt}^2)P_0 \quad (2)$$

where x_{water} and x_{salt} are the molar fraction of water and salt in the feed and distillate solution, and P_0 is the vapour pressure of pure water, which can be calculated using the Antoine equation [2, 13]:

$$P_0 = exp(23.1964 - \frac{3816.44}{T-46.13}) \quad (3)$$

where T is the temperature (K) of the feed and distillate at the membrane surface.

The membrane mass transfer coefficient (C_m) is dependent on membrane properties and process operating conditions. For seawater desalination by DCMD, C_m can be described as [13, 17, 32, 33]:

$$C_m = \left[\frac{3}{2}\frac{\tau\delta}{\varepsilon r}\left(\frac{\pi RT}{8M}\right)^{1/2} + \frac{\tau\delta}{\varepsilon}\frac{P_a}{PD}\frac{RT}{M}\right]^{-1} \quad (4)$$

where δ, ε, τ, and r are the membrane thickness (m), porosity (dimensionless), pore tortuosity (dimensionless), and pore radius (m), respectively, M is the molecular weight of water (kg/mol), R is the gas constant (i.e. 8.314 J/(mol·K)), T is the mean water vapour temperature (K) inside the membrane pore, P and P_a are the total pressure and the air partial pressure (Pa) inside the membrane pore, and D is the water diffusion coefficient (m^2/s). The multiplication of P and D is a function of temperature, and can be calculated as:

$$PD = 1.895\times10^{-5}T^{2.072} \quad (5)$$

The heat flux (Q) through the membrane is a combination of conduction heat and latent heat, and can be described as:

$$Q = \frac{k_m}{\delta}\left(T_{m.f} - T_{m.d}\right) + J\Delta H_v \quad (6)$$

where Q is in kJ/(m^2·h), k_m is the membrane thermal conductivity (W/(m·K)), ΔH_v is the latent heat of evaporation (kJ/kg), and $T_{m.f}$ and $T_{m.d}$ are the temperatures of the feed and distillate streams at the membrane surfaces, respectively. The membrane thermal conductivity is the volume-average of polymer thermal conductivity (k_s) and gas thermal conductivity (k_g) as follows [34]:

$$k_m = \left[\frac{\varepsilon}{k_g} + \frac{1-\varepsilon}{k_s}\right]^{-1} \quad (7)$$

The procedure to calculate k_s and k_g is available from Alkhudhiri et al. [13]. ΔH_v is calculated using the mean water vapour temperature inside the membrane pore as:

$$\Delta H_v = 1.7535T + 2024.3 \quad (8)$$

The temperature of the feed and distillate streams at the membrane surfaces (i.e. $T_{m.f}$ and $T_{m.d}$) can be determined based on the bulk stream temperatures (i.e. $T_{b.f}$ and $T_{b.d}$) by iteration as follows [35, 36]:

$$T_{m.f} = \frac{T_{b.f}h_f + h_m\left(T_{b.d} + T_{b.f}\dfrac{h_f}{h_d}\right) - J\Delta H_v}{h_f\left(1 + \dfrac{h_m}{h_d}\right) + h_m} \quad (9)$$

$$T_{m.d} = \frac{T_{b.d}h_d + h_m\left(T_{b.f} + T_{b.d}\dfrac{h_d}{h_f}\right) + J\Delta H_v}{h_d\left(1 + \dfrac{h_m}{h_f}\right) + h_m} \quad (10)$$

where h_f and h_d are the heat transfer coefficients in the feed and distillate thermal boundary layers respectively, and h_m is the heat transfer coefficient across the membrane. The calculation of the heat transfer coefficients in the boundary layers (h_f and h_d) involves the Nusselt number (Nu):

$$h_{f,d} = \frac{Nu_{f,d}k}{d_h} \quad (11)$$

where k is the thermal conductivity (W/(m·K)) of the feed and distillate streams, and d_h is the hydraulic diameter of the feed and distillate channels. For a flat sheet DCMD module at laminar flow, Nu can be calculated as [36, 37]:

$$Nu = 0.097 Re^{0.73} Pr_b^{0.13} \left(\frac{Pr_b}{Pr_m} \right)^{0.25} \quad (12)$$

where Re is the Reynolds number, Pr is the Prandtl number, and the subscripts b and m represent bulk fluid and membrane surface, respectively. The calculations of Re and Pr are as follows:

$$Re = \frac{\rho u d_h}{\mu} \quad (13)$$

$$Pr = \frac{\mu C_p}{k} \quad (14)$$

where ρ, μ, and C_p are density (kg/m^3), dynamic viscosity (kg/(m·s)), and specific heat capacity (kJ/(kg·K)) of the feed and distillate streams, and u is the fluid cross flow velocity (m/s).

During the DCMD process, temperature polarisation effect renders the temperature difference between the hot and cold membrane surfaces smaller than that between the bulk feed and distillate streams, thus reducing the actual process driving force. The temperature polarisation coefficient (Φ) is calculated as:

$$\Phi = \frac{T_{m.f} - T_{m.d}}{T_{b.f} - T_{b.d}} \quad (15)$$

In the DCMD process, temperature and concentration polarisation can occur simultaneously. Because the influence of concentration polarisation on water flux is insignificant compared to that of temperature polarisation during the desalination of seawater by DCMD [4, 13, 32], concentration polarisation is excluded in this study.

Thermal efficiency (Π) is an important parameter to evaluate the performance of DCMD. Π is the ratio of the latent heat over the total heat flux through the membrane and can be calculated as:

$$\Pi = \frac{J \Delta H_v}{J \Delta H_v + \frac{k_m}{\delta} (T_{m.f} - T_{m.d})} \quad (16)$$

3. Computer software package and process simulation

3.1. TRNSYS simulation package

The Transient System Simulation (TRNSYS) software package version 17.2 was used to simulate an integrated solar thermal driven DCMD system. Accredited built-in components including a flat plate solar thermal collector (Type 539), a water pump (Type 3b), an online plotter (Type 65c), and weather data reading and processing (Type 15-3) in the TRNSYS library were used without any modification. Other components including a spiral-wound DCMD module, a feed tank, and controllers were composed by the authors. The solar thermal collector (i.e. composed of 10 flat panels in series) had an effective surface area A of 22.6 m^2, intercept efficiency a_0 of 0.687, the 1st order and the 2nd order efficiency coefficients a_1 and a_2 of 1.505 and 0.0111, respectively.

A spiral-wound DCMD module from AquaStill (Sittard, The Netherlands) was chosen for the simulation. The DCMD module had 6 feed and distillate parallel channels, each of which had height, width, and length of 2 mm and 0.4 m, and 1.5 m, respectively [38]. The total membrane surface area was 7.2 m^2 [38]. According to the manufacturer, the water circulation flowrates of this module were from 600 to 1500 L/h (equivalent to 3.5 to 8.7 cm/s in cross flow velocities) [38]. The initial water volume of the feed tank was set at 3 m^3. Hourly recorded weather data from 1st to 5th January 1991 for a coastal location (-33.87° N; 151.20° E) in New South Wales Australia were arbitrarily selected as solar radiation input for the simulation.

3.2. Process simulation

The flow directions and descriptions of heat and mass transfer in the DCMD membrane module under co-current and counter-current flow are illustrated in Fig. 1. For both flow modes, the mass flux of water (J_i) through an incremental membrane area i is calculated using Eqs. (1-5) with $T_{m.f.i}$ and $T_{m.d.i}$ determined via the mathematical iterative models (Eqs. 9 & 10). Then, the mass flow of water from the feed to the distillate (dm_i) can be calculated as:

$$dm_i = J_i W dx \tag{17}$$

where dm_i is in kg/h, W is the width of the flow channels (m), and dx is the incremental membrane length (m). The heat flux through the membrane area Wdx is:

$$dQ_i = \left(J_i \Delta H_v + \frac{k_m}{\delta} (T_{m.f} - T_{m.d}) \right) W dx \tag{18}$$

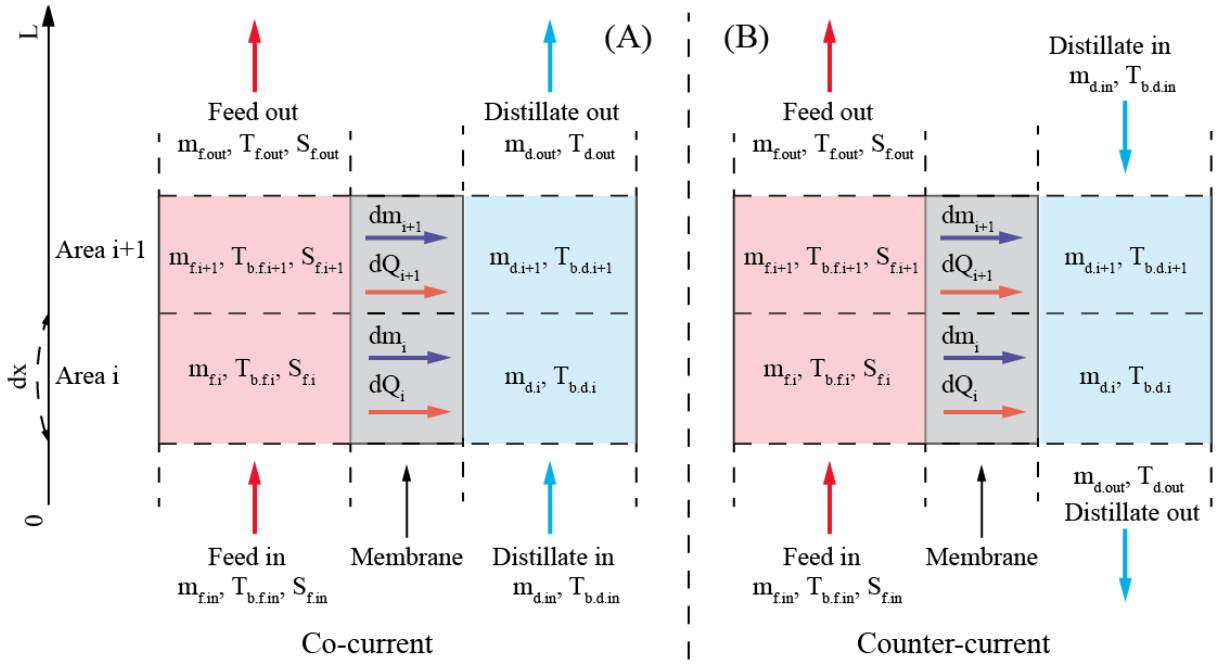

Fig. 1. Schematic diagram of two incremental membrane areas along the DCMD module under the (A) co-current and (B) counter-current flow mode.

From mass and heat balance, the mass flow (m_f), bulk temperature ($T_{b.f}$), and salinity (S_f) of the feed stream at the area *i+1* can be determined as follows:

$$m_{f.i+1} = m_{f.i} - dm_i \tag{19}$$

$$S_{f.i+1} = \frac{m_{f.i} S_{f.i}}{m_{f.i+1}} \tag{20}$$

$$T_{b.f.i+1} = \frac{m_{f.i} Cp_{f.i} T_{b.f.i} - dQ_i}{m_{f.i+1} Cp_{f.i}} \tag{21}$$

The mass flow (m_d) and the bulk temperature ($T_{b.d}$) of the distillate stream at the area *i+1* under co-current flow are calculated as:

$$m_{d.i+1} = m_{d.i} + dm_i \tag{22}$$

$$T_{b.d.i+1} = \frac{m_{d.i} Cp_{d.i} T_{b.d.i} + dQ_i}{m_{d.i+1} Cp_{d.i}} \tag{23}$$

For counter-current flow, these parameters are determined as follows:

$$m_{d.i+1} = m_{d.i} - dm_i \tag{24}$$

$$T_{b.d.i+1} = \frac{m_{d.i} Cp_{d.i} T_{b.d.i} - dQ_i}{m_{d.i+1} Cp_{d.i}} \quad (25)$$

For simplicity, it is assumed that: (1) the system is at steady state; (2) the feed and the distillate streams only flow in the *x* direction; (3) salt rejection is 100%; and (4) there is no heat loss to the environment.

The calculation algorithms of the DCMD process are provided in Fig. 2 and Fig. 3 for co-current and counter-current, respectively. The calculation starts from the feed inlet end (i.e. x_0 = 0) and finishes at the feed outlet end (i.e. $x_n = L$) of the DCMD module. For co-current flow, the initial parameters of the feed and distillate streams are readily available. On the other hand, for counter-current flow, initial guesses of the mass flow and temperature of the distillate at the outlet (i.e. $m_{d.out}$ and $T_{d.out}$) are required (Fig. 3).

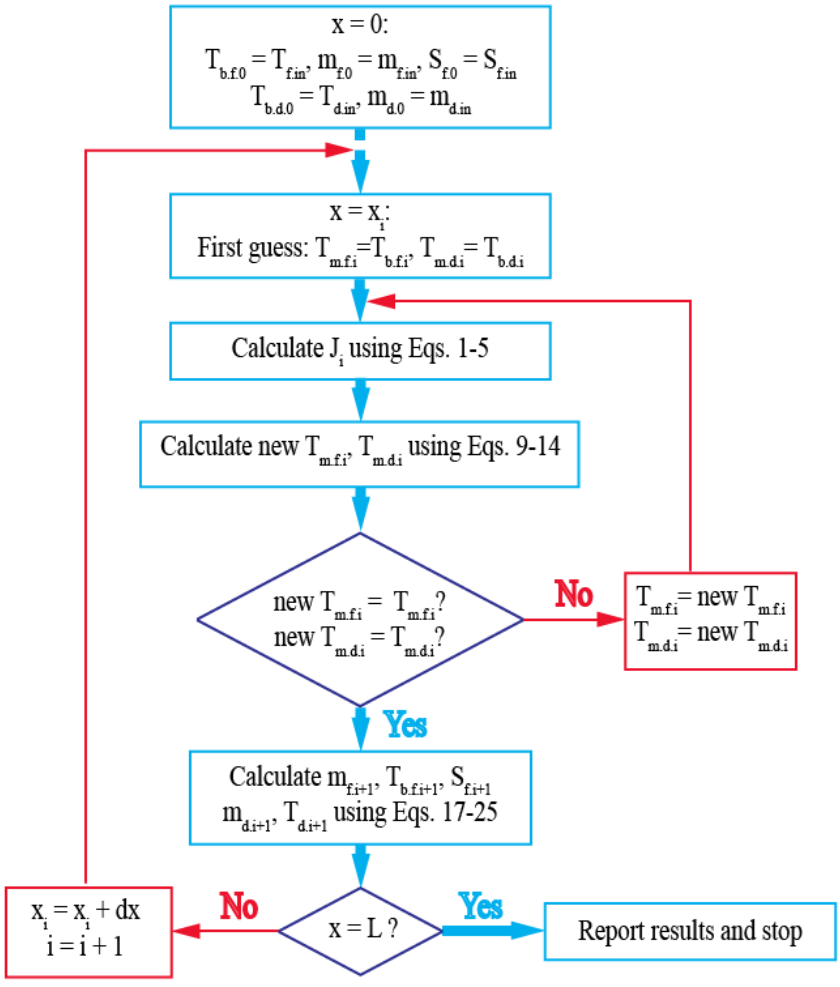

Fig. 2. Calculation algorithm of the DCMD model for co-current flow.

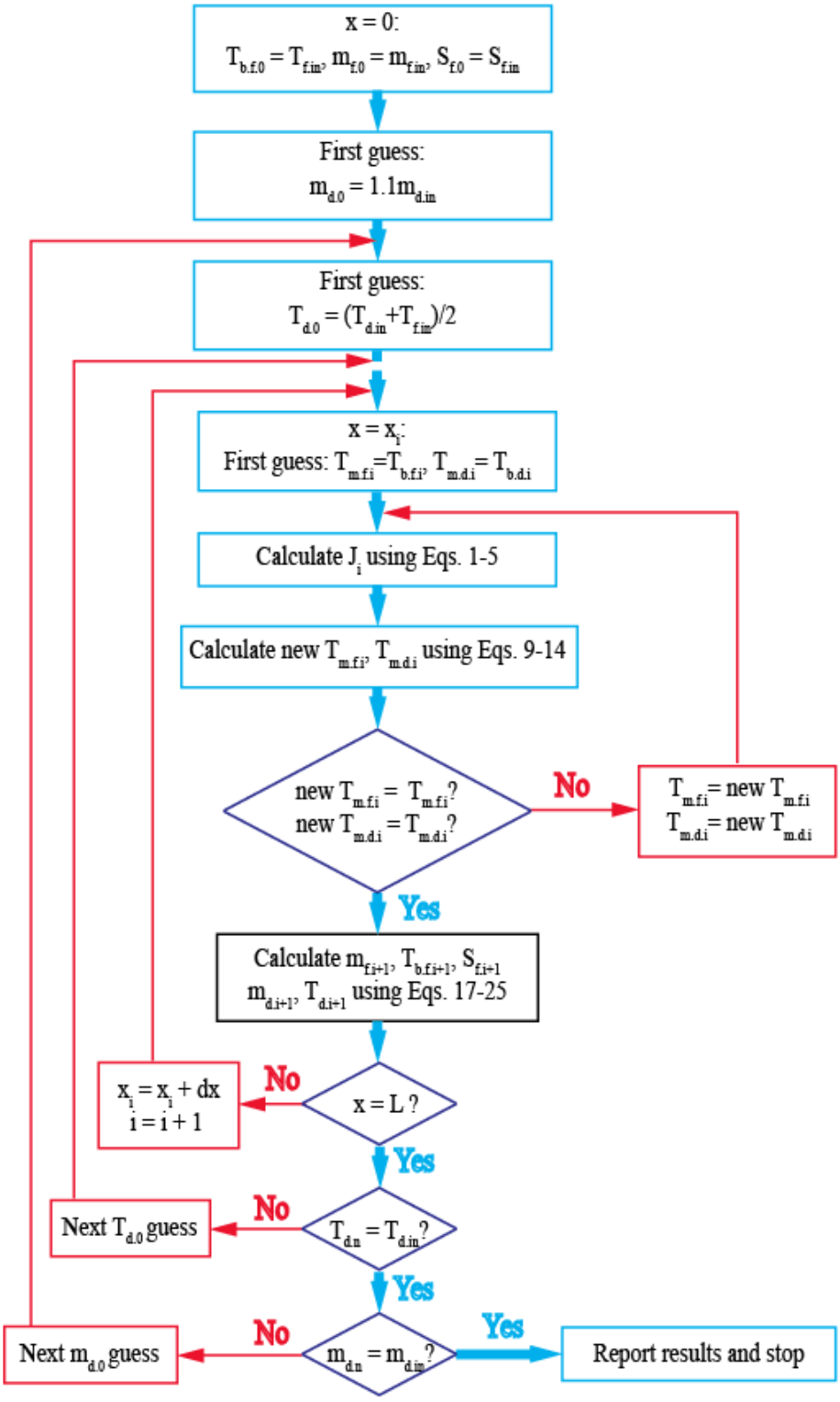

Fig. 3. Calculation algorithm of the DCMD model for counter-current flow.

In the solar thermal driven DCMD system under brine-recycled operation, seawater is circulated through the solar thermal collector to the DCMD module and back to the feed tank (Fig. 4). Within the DCMD module, distillate is collected and the feed seawater is concentrated.

Thus, the feed water mass (m_{tank}), salinity (S_{tank}), and temperature (T_{tank}) in the feed tank change with operating time. Their values at two consecutive simulation steps (i.e. j and $j+1$) are calculated as:

$$S_{tank.j+1} = \frac{S_{tank.j} m_{tank.j}}{m_{tank.j} - F_{MD.dist}} \quad (26)$$

$$T_{tank.j+1} = \frac{F_{MD.brine} T_{MD.brine} + (m_{tank.j} - F_{MD.feed}) T_{tank.j}}{m_{tank.j} - F_{MD.dist}} \quad (27)$$

$$m_{tank.j+1} = m_{tank.j} - F_{MD.dist} \quad (28)$$

where $F_{MD.dist}$ is the distillate production rate (kg/h) of the DCMD module, $F_{MD.brine}$ and $T_{MD.brine}$ are the mass flow (kg/h) and temperature (°C) of the brine leaving the DCMD module respectively, and $F_{MD.feed}$ is the mass flow of the feed water into the DCMD module.

Under the single-pass operation, the concentrated brine leaving the DCMD membrane module is discharged from the system (Fig. 4); thus, the feed water temperature and salinity remain unchanged.

During the solar thermal driven DCMD process, heat loss to the environment from the solar thermal collector, the membrane module, the feed tank, and piping can occur [30]. Heat loss from the solar thermal collector is embedded in its efficiency coefficients (e.g. *a1* and *a2*). For simplicity, it is assumed that the system can be fully insulated and heat loss from other system components is negligible.

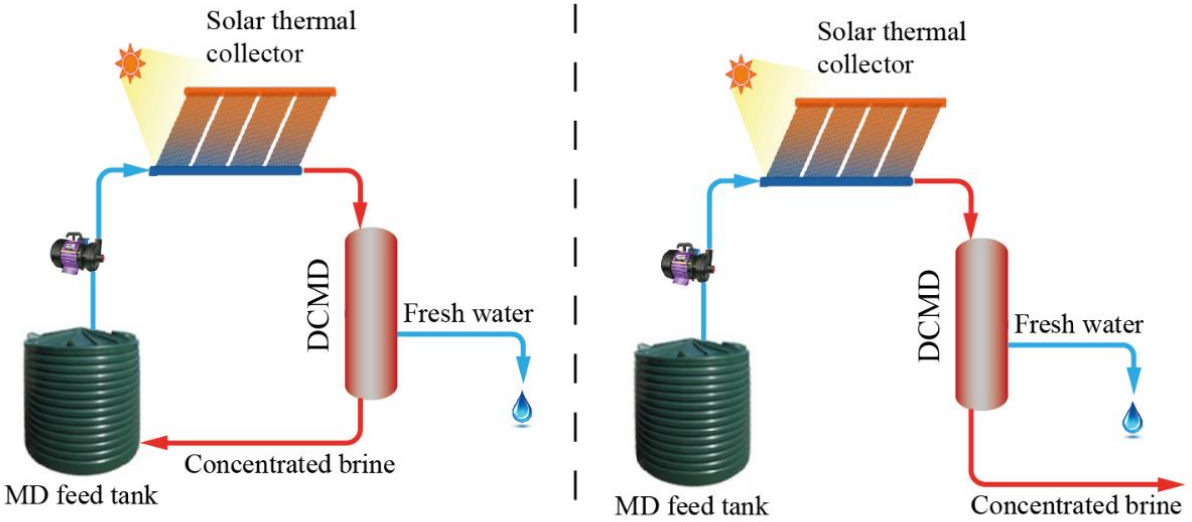

A brine-recycled DCMD process

A single-pass DCMD process

Fig. 4. Schematic diagram of a brine-recycled and a single-pass solar thermal DCMD process.

4. Results and discussions

4.1. Mass and heat transfer within the DCMD module

Co-current and counter-current flow result in two distinctive temperature profiles along the channel length (Fig. 5). In the co-current flow, the feed temperature decreases while the distillate temperature increases, resulting in a continuous decrease in the temperature difference (ΔT) between the feed and distillate channels along the membrane module. In contrast, in the counter-current flow, the feed and distillate temperatures decrease at a similar rate; thus, ΔT is relatively constant along the channel length (Fig. 5).

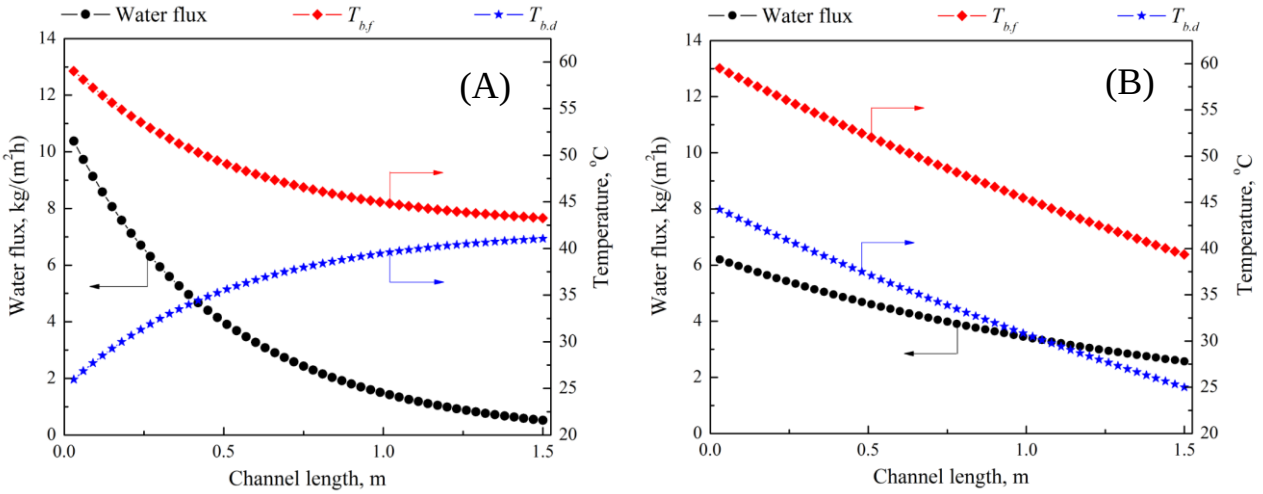

Fig. 5. Water flux, bulk feed temperature ($T_{b.f}$), and bulk distillate temperature ($T_{b.d}$) along the DCMD module channels under (A) co-current and (B) counter-current flow. Operating conditions: feed inlet temperature, $T_{f.in}$ = 60 °C; distillate inlet temperature, $T_{d.in}$ = 25 °C; feed and distillate cross flow velocities of 5.2 cm/s (i.e. equivalent to process water circulation rates of 900 L/h); feed inlet salinity, $S_{f.in}$ = 35,000 ppm.

The difference in ΔT behaviour along the channel length results in two distinctive water flux profiles under the two flow modes (Fig. 5). In the co-current flow, water flux decreases rapidly along the channel length as a result of the reduction in ΔT between the feed and distillate streams (Fig. 5A). Due to the exponential relationship between water vapour pressure and temperature (Eq. 3), water flux decreases at a faster rate than the decline in ΔT in the co-current flow. Indeed, between the module inlet and outlet, water flux decreases by 20 times whereas ΔT only decreases by 12 times (Fig. 5A). Under the counter-current flow mode, a gradual decrease in water flux is observed despite a constant ΔT along the channel length (Fig. 5B). This is because the water

vapour partial pressure difference between the feed and distillate channels depends not only on ΔT but also the temperature of the feed.

According to Eq. 9 and Eq. 10, temperature polarisation is reduced when the water flux decreases. Thus, for both flow modes, temperature polarisation coefficient (Φ) increases along the channel length (Fig. 6A). It is noteworthy that Φ values from this (Fig. 6A) and other modelling investigations [24, 39] are lower than those obtained in experimental studies using lab-scale DCMD modules (i.e. Φ >0.8) [40-42]. This is because lab-scale experimental studies are often based on operating parameters (e.g. high feed/distillate cross flow velocities and small membrane surface area) that are not realistic for pilot or full-scale operations.

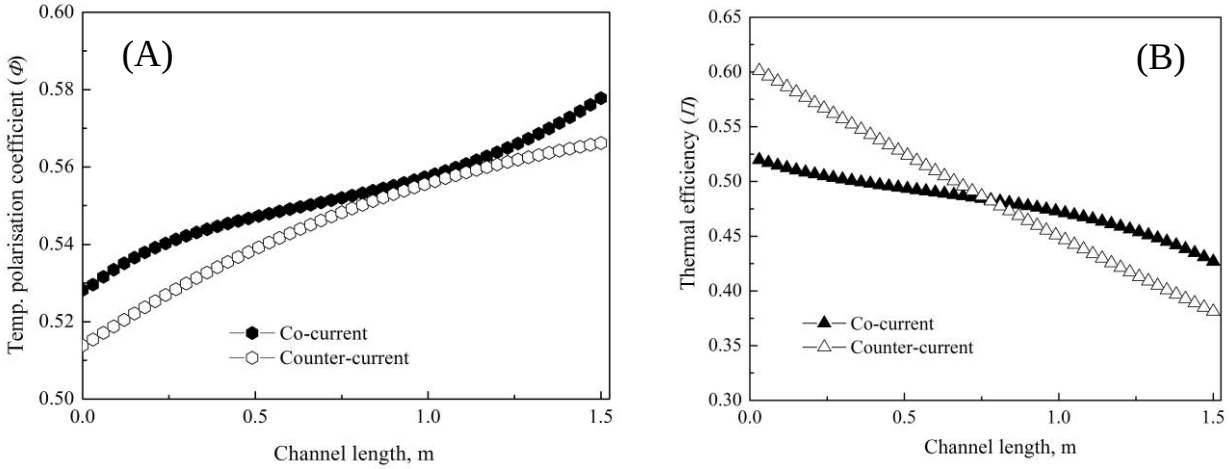

Fig. 6. Simulated temperature polarisation coefficient (Φ) and thermal efficiency (Π) along the DCMD module channels under co-current and counter-current flow. Operating conditions: feed inlet temperature, $T_{f.in}$ = 60 °C; distillate inlet temperature, $T_{d.in}$ = 25 °C; feed and distillate cross flow velocities of 5.2 cm/s (process water circulation rates of 900 L/h); feed inlet salinity, $S_{f.in}$ = 35,000 ppm.

Thermal efficiency (Π) decreases along the channel length under both co-current and counter-current flow modes (Fig. 6B). At the feed inlet, Π is 0.52 and 0.60 under co-current and counter-current flow, respectively. At the feed outlet, Π decreases to 0.43 for co-current flow and to 0.38 for counter-current flow. It has been established that operating the DCMD process at a higher feed temperature increases the process thermal efficiency [43-45]. Thus, the decrease in Π can be attributed to the declined feed temperature along the channel length (Fig. 5).

4.2. Performance of the DCMD module

The relationships between water flux and thermal efficiency with feed temperature at the module level are demonstrated in Fig. 7. These results are consistent with the data presented in the previous section. It is interesting to note that under the two flow modes, the DCMD module

exhibits similar thermal efficiency but different water flux, particularly at high feed inlet temperatures (Fig. 7). The divergence in the module water flux between the two flow modes at high feed inlet temperatures is attributed to the ΔT variation along the module channels (Fig. 5). Under counter-current flow, at a high feed inlet temperature, a large ΔT value can be obtained and maintained along the membrane module, resulting in a high module water flux. On the other hand, under co-current flow, a high feed inlet temperature results in a large ΔT only at the module entrance, and ΔT decreases rapidly along the membrane module. As a result, the overall module water flux under co-current is lower than that under counter-current flow (Fig. 7).

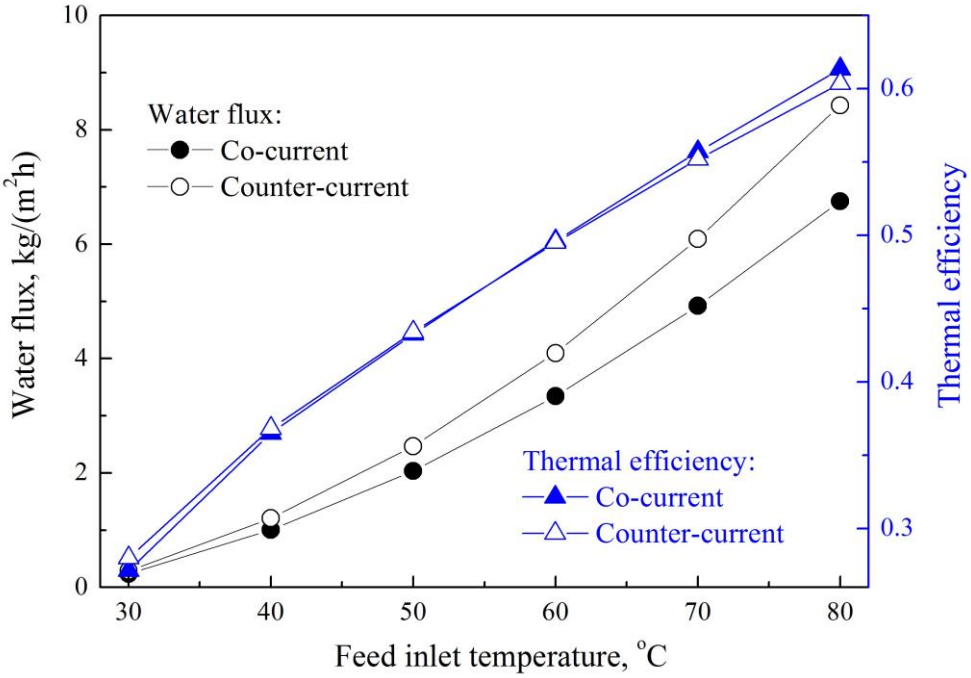

Fig. 7. Influences of feed inlet temperature on the water flux and thermal efficiency of the DCMD module under co-current and counter-current flow. Other operating conditions: distillate inlet temperature, $T_{d.in}$ = 25 °C; feed and distillate cross flow velocities of 5.2 cm/s (process water circulation rates of 900 L/h); feed inlet salinity, $S_{f.in}$ = 35,000 ppm. The DCMD module has 1.5 m long channels.

Increasing water cross flow velocities in the feed and distillate channels leads to an increase in ΔT, thus improving both the module water flux and thermal efficiency (Fig. 8). Indeed, the simulation results show that increasing water cross flow velocities from 3.5 to 8.7 cm/s doubles the average ΔT under both co-current and counter-current flow modes. Moreover, increasing the cross flow velocities in the feed and distillate channels can also reduce the temperature polarisation effect within the DCMD module. As the cross flow velocities of the feed and distillate channels increase from 3.5 to 8.7 cm/s, the average temperature polarisation coefficient

(Φ) of the DCMD module at the feed inlet temperature of 60 °C increases from 0.49 to 0.64 under both co-current and counter-current flow modes.

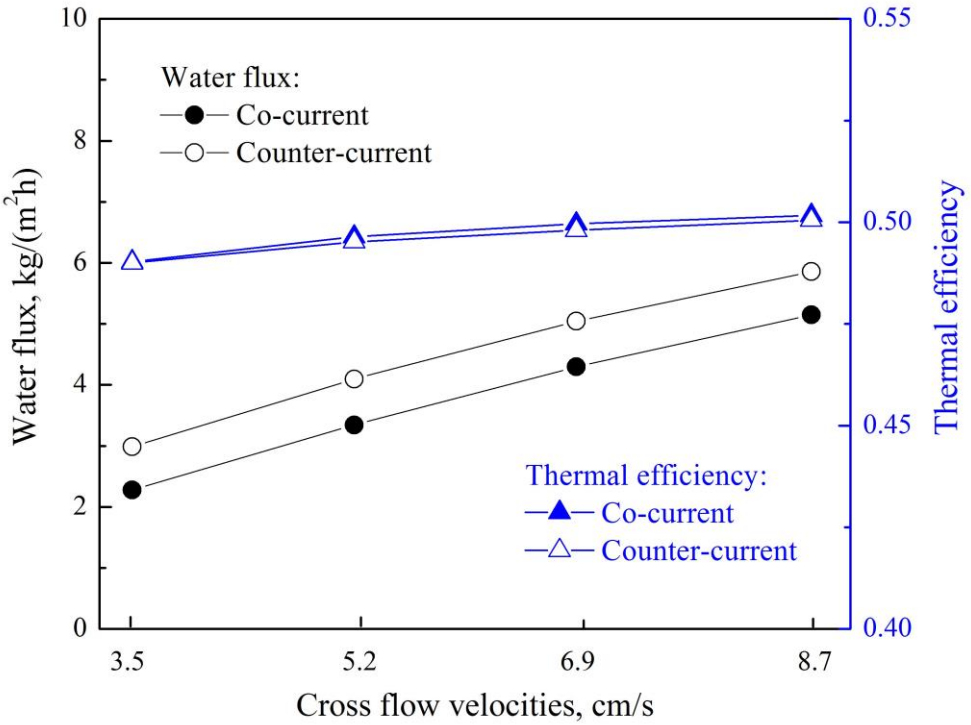

Fig. 8. Influences of water cross flow velocities on the water flux and thermal efficiency of the DCMD module under co-current and counter-current flow. Other operating conditions: feed inlet temperature, $T_{f.in}$ = 60 °C; distillate inlet temperature, $T_{d.in}$ = 25 °C; feed inlet salinity, $S_{f.in}$ = 35,000 ppm. The DCMD module has 1.5 m long channels.

The influences of water cross flow velocities on water flux and thermal efficiency of the DCMD membrane module are much smaller than those of feed inlet temperature. Increasing water cross flow velocities by 2.5 times (i.e. from 3.5 to 8.7 cm/s) results in an increase of the same magnitude in the module water flux and a slight improvement in the module thermal efficiency (Fig. 8). On the other hand, increasing feed inlet temperature from 30 to 80 °C exponentially raises the module water flux, and markedly increases the module thermal efficiency (Fig. 7). These results have an important implication on the optimisation of a solar thermal driven DCMD system. Indeed, when the supply of solar thermal is limited, increased feed water cross flow velocities can significantly reduce the DCMD feed inlet temperature. Thus, in an integrated system, increasing the cross flow velocities might even be counter-productive. The influence of water cross flow velocities on water flux and thermal efficiency of the solar thermal driven DCMD process will be discussed in the section 4.3.

The simulation results reported here provide two important implications towards process optimisation of a solar thermal driven DCMD system for seawater desalination. First, under the

operating conditions investigated in this study, the DCMD module exhibits similar thermal efficiency under co-current and counter-current flow modes; however, counter-current flow results in a higher water flux. Thus, counter-current flow is preferable to co-current flow when the supply of thermal energy is limited. Second, the hot brine (i.e. at 40 °C for the feed inlet temperature of 60 °C under counter-current flow) leaving the membrane module has a considerable amount of sensible heat. Indeed, Duong et al. [46] have experimentally demonstrated the benefits of brine recycling in the DCMD process with respects to thermal efficiency. Thus, by simply recycling the hot brine to the module, this sensible heat can be recovered to enhance the overall thermal performance of the DCMD process. The next section analyses the performance of a solar thermal driven DCMD process with brine recycling under real weather conditions.

4.3. Performance of a solar thermal driven DCMD process

A solar thermal driven DCMD system consisting of a 7.2 m^2 membrane module under counter-current flow and 22.6 m^2 of flat plate solar thermal collector was simulated using TRNSYS. The results show a highly intermittent nature of the solar thermal driven DCMD process. The process achieves maximum water flux and thermal efficiency when the feed inlet temperature reaches the highest value at peak solar radiation (Fig. 9). On the hottest day of the operation (i.e. the 2^{nd} day), the system under brine-recycled operation obtains the maximum water flux of 2.7 kg/(m^2·h) at peak feed inlet temperature of 52 °C (i.e. coinciding with the peak total solar radiation of 1100 W/m^2), and produces 142 kg of distillate for the day. This daily distillate production rate is equivalent to 19.7 kg/day per 1 m^2 of DCMD membrane and 6.3 kg/day per 1 m^2 of solar thermal collector. The overall thermal efficiency of the system varies from 0 (in early morning and late afternoon) to about 0.5 (at peak solar radiation).

Results from our simulation are comparable to the data from several previous pilot studies (Table 1). Compared to these pilot scale data, the simulated solar thermal driven DCMD system achieves a higher daily distillate production rate per 1 m^2 of membrane. On the other hand, in terms of the collector area, the simulated daily distillate production rate is lower when comparing to the data experimentally obtained from pilot operation (Table 1). These differences are attributed to the higher water flux but lower thermal efficiency of DCMD as compared to AGMD and PGMD. It is noteworthy that no previous pilot scale solar thermal driven DCMD studies are available for a direct comparison.

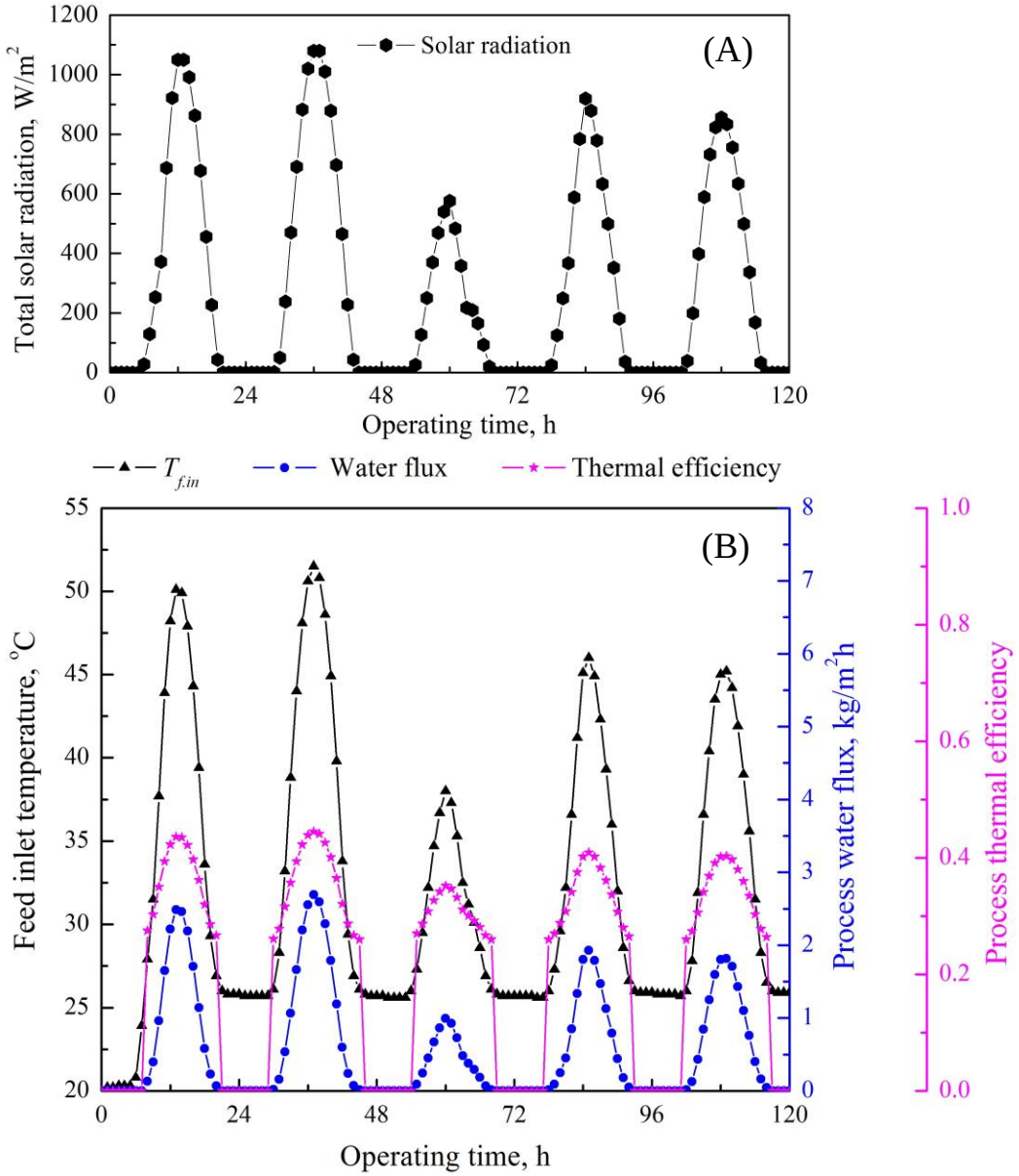

Fig. 9. Variations in (A) the total solar radiation, and (B) the feed inlet temperature ($T_{f.in}$), water flux, and thermal efficiency of the solar thermal driven DCMD process during a brine-recycled operation. Operating conditions: $T_{d.in}$ = *25* °C, water cross flow velocities in DCMD channels of 5.2 cm/s (i.e. equivalent to process water circulation rates of 900 L/h). The simulation data are for the 1st to the 5th of January 1991.

Table 1. Comparisons between the simulated DCMD system and the data from pilot operations of solar thermal driven MD systems in the literature.

	Simulated data from this study	Pilot data from the literature		
		[18]	[19]	[20]
Configurations	DCMD	PGMD	PGMD	AGMD
Membrane area (m^2)	7.2	10	–	8
Thermal collector area (m^2)	22.6	5.73	5.73	5.9
Daily distillate production (kg/d)	142	<120	64.17	81
Distillate production/membrane area (kg/(m^2·d) membrane)	19.7	<12.0	–	10.13
Distillate production/collector area (kg/(m^2·d) collector)	6.3	<20.9	11.2	13.7

Our simulation data highlight the need to consider MD operation together with the source of thermal energy. Unlike the results in section 4.2 when the DCMD module is considered independently of the energy source, in an integrated system, increasing the DCMD water cross flow velocities from 3.5 to 8.7 cm/s decreases the maximum water flux and thermal efficiency at peaked hours from 3.2 to 2.5 kg/(m^2·h) and from 0.48 to 0.41, respectively (Fig. 10). This is because the feed inlet temperature is no longer independent from the feed cross flow velocity. Increasing feed cross flow velocity shortens the residence time of the feed within the thermal collector, thus leading to a decrease in DCMD feed inlet temperature (Fig. 10). Operating the solar thermal DCMD process at low cross flow velocities is beneficial with respects to water flux and thermal efficiency. However, the seawater DCMD process at low cross flow velocities might be strongly affected by concentration polarisation effect and membrane scaling at high process water recoveries [46, 47]. Thus, further simulations of the solar thermal driven seawater DCMD process that take account of concentration polarisation effect and membrane scaling are recommended.

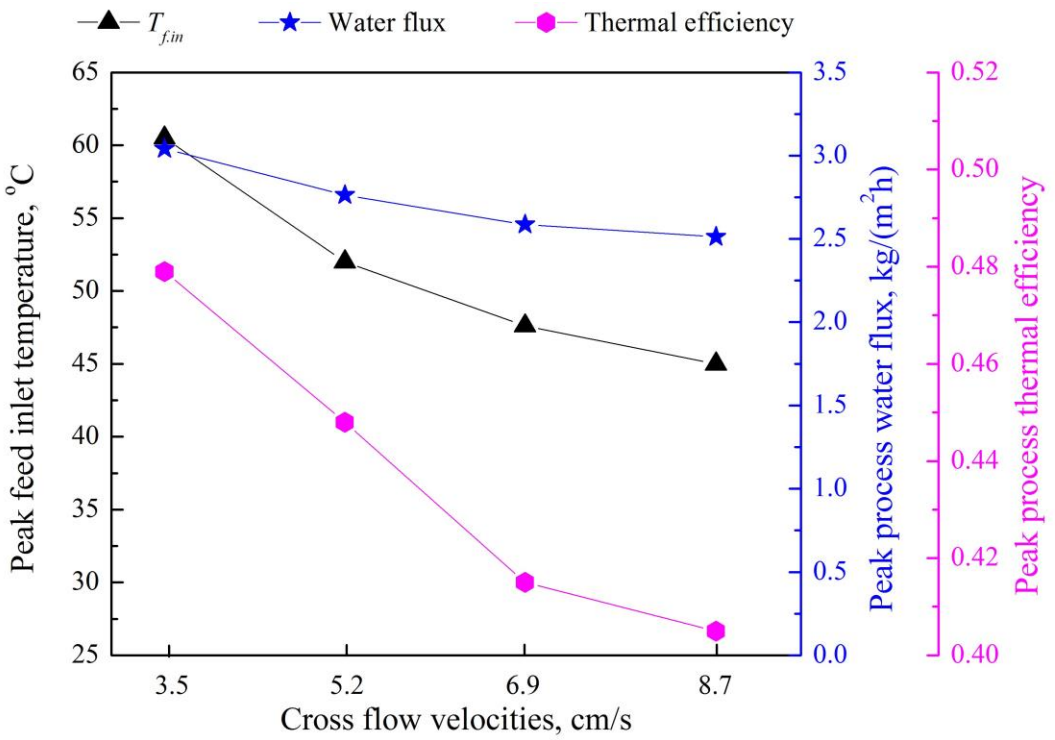

Fig. 10. Influence of water cross flow velocities on the feed inlet temperature, water flux, and thermal efficiency of the solar thermal driven DCMD process at peak solar radiation. Operating conditions: $T_{d.in}$ = *25* °C. The simulation data are for the 2nd of January 1991.

The simulation data also confirm the benefits of brine recycling during the solar thermal driven seawater DCMD desalination process (Fig. 11). Returning the warm brine to the feed tank in lieu of discharging it from the process recovers the sensible heat of the brine [30, 46], thus elevating the temperature of the feed water in the feed tank. The warmer is the feed water in the feed tank, the hotter feed water can be obtained at the outlet of the solar thermal collector. As demonstrated in Fig. 11A, during a single-pass operation at water cross flow velocities of 5.2 cm/s, the peak collector outlet temperature is 40 °C (i.e. with seawater feed temperature of 25 °C), whereas the brine-recycled operation achieves the peak collector outlet temperature of 52 °C. As a result, the peak water flux of the brine-recycled solar thermal driven DCMD process significantly increases to 2.7 kg/(m^2·h) as compared to 1.2 kg/(m^2·h) obtained in a single-pass process (Fig. 11B). Accordingly, the peak process thermal efficiency also increases from 0.35 to 0.45 when the operation mode is switched from single-pass to brine-recycled (Fig. 11C).

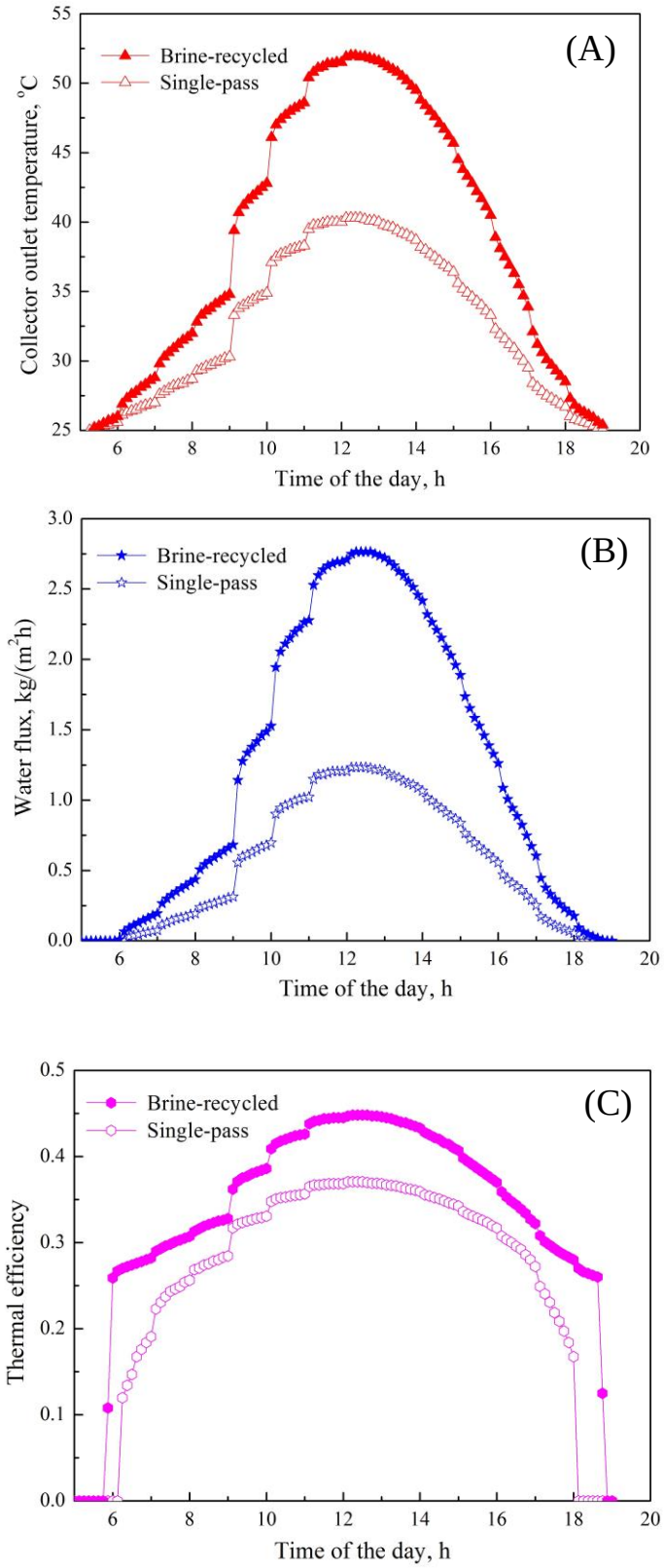

403 **Fig. 11.** (A) thermal collector outlet temperature, (B) water flux, and (C) thermal efficiency of the
404 solar thermal driven DCMD process during the daytime at two operation modes: single-pass and
405 brine-recycled. Operating conditions: $T_{d.in}$ = *25* °C, water cross flow velocities in DCMD

channels of 5.2 cm/s (i.e. equivalent to process water circulation rates of 900 L/h). The simulation data are for the 2nd of January 1991.

In addition to the water cross flow velocity and operation mode, other design factors such as sizes of the MD feed tank, the solar thermal collector, and the MD membrane module as well as solar radiation condition can exert strong influences on water flux and thermal efficiency of the solar thermal DCMD system. Reducing the MD feed tank volume leads to an increase in the feed water temperature (Eq. 27) and the collector outlet temperature, thus increasing the system water flux and thermal efficiency [29]. Increasing the solar thermal collector area can improve the system performance but requires a higher capital expenditure. It is noted that simulation results from this study are from optimistic solar radiation condition. On a typical winter day (i.e. the 1st of July), under brine-recycled operation, the simulated peak water flux and thermal efficiency are 1.4 kg/(m^2·h) and 0.24, respectively.

5. Conclusions

Computer simulations were conducted to assess the performance of an integrated solar thermal driven seawater DCMD system. The results show that DCMD operation under co-current and counter-current flow results in two distinctive profiles in water flux, temperature polarisation effect, and thermal efficiency along the channel length. Although, under the two flow modes, similar thermal efficiency was obtained, the counter-current flow mode is preferable over co-current with respects to water flux, particularly at high feed operating temperatures. More importantly, the simulated data highlight the need to consider the DCMD process together with the source of thermal energy. When considered in isolation from the supply of thermal energy, increasing water cross flow velocities inside the module channels increases the overall water flux and thermal efficiency of the DCMD membrane module. However, when the membrane module is coupled with the solar thermal collector, increasing the feed and distillate cross flow velocities reduces the water flux and thermal efficiency. Using previously recorded weather data, it is shown that, each day a solar thermal driven DCMD system with brine recycling can produce 19.7 kg of clean water per m^2 of membrane or 6.3 kg of clean water per m^2 solar thermal collector.

Nomenclature

C_m	Membrane mass transfer coefficient, kg/(m^2·h·Pa)
C_p	Specific heat capacity, kJ/(kg·K)
D	Water diffusion coefficient, m^2/s
dm	Water mass flow through an incremental membrane area, kg/h

d_h	Hydraulic diameter of the module channels, m
dQ	The heat flux through an incremental membrane area, kJ/h
dx	The length of an incremental membrane area, m
$F_{MD.brine}$	The MD brine mass flow, kg/h
$F_{MD.feed}$	The feed stream mass flow, kg/h
$F_{MD.dist}$	Distillate production rate, kg/h
h_d	Mass transfer coefficient of the distillate stream, W/m^2·K
h_m	Mass transfer coefficient of the membrane, W/m^2·K
h_f	Mass transfer coefficient of the feed stream, W/m^2·K
i	Incremental membrane area index
J	Water flux, kg/(m^2·h)
j	Simulation step
k_g	Gas thermal conductivity, W/(m·K)
k_m	Membrane thermal conductivity, W/(m·K)
k_s	Membrane polymer thermal conductivity, W/(m·K)
L	Membrane module channel length, m
M	Molecular weight of water, kg/mol
m_d	Distillate mass flow, kg/h
m_f	Feed mass flow, kg/h
m_{tank}	The mass of water in the MD feed tank, kg
Nu	Nusselt number
P	Total pressure inside membrane pores, Pa
P_a	Partial pressure of air inside membrane pores, Pa
$P_{m.f}$	Water vapour pressure at the feed membrane surface, Pa
$P_{m.d}$	Water vapour pressure at the distillate membrane surface, Pa
P_0	Water vapour pressure of pure water, Pa
Pr	Prandtl number
Pr_b	Prandtl number in the fluid
Pr_m	Prandtl number at the membrane surface
Q	Heat flux through the membrane, kJ/(m^2·h)
R	Universal gas constant, J/(mol·K)
Re	Reynolds number
r	Membrane pore radius, m
$S_{f.in}$	Feed inlet salinity, ppm
$S_{f.out}$	Feed outlet salinity, ppm
S_{tank}	Salinity of water in the MD feed tank, ppm
T	Mean water vapour temperature inside the membrane pores, K
$T_{b.d}$	Temperature in the bulk distillate stream, K
$T_{b.f}$	Temperature in the bulk feed stream, K
$T_{m.d}$	Temperature at the distillate membrane surface, K
$T_{m.f}$	Temperature at the feed membrane surface, K
u	Fluid cross flow velocity, m/s
W	Flow channel width, m
x_{salt}	Molar fraction of salt
x_{water}	Molar fraction of water

Greek symbols

δ	Membrane thickness, m
ε	Membrane porosity
τ	Membrane pore tortuosity
μ	Dynamic viscosity, kg/(m·s)
ΔH_v	Latent heat of evaporation, kJ/kg

Acknowledgments

The Vietnam International Education Development (VIED), under the Ministry of Education and Training (MoET), and the University of Wollongong (UOW) are acknowledged for PhD scholarship support to Hung C. Duong.

References

1. E. Drioli, A. Ali, and F. Macedonio, Membrane distillation: Recent developments and perspectives, Desalination 356 (2015) 56-84.
2. K.W. Lawson and D.R. Lloyd, Membrane distillation, J. Membr. Sci. 124 (1997) 1-25.
3. L.D. Nghiem and T. Cath, A scaling mitigation approach during direct contact membrane distillation, Sep. Purif. Technol. 80 (2011) 315-322.
4. S. Adham, A. Hussain, J.M. Matar, R. Dores, and A. Janson, Application of membrane distillation for desalting brines from thermal desalination plants, Desalination 314 (2013) 101-108.
5. J.-P. Mericq, S. Laborie, and C. Cabassud, Evaluation of systems coupling vacuum membrane distillation and solar energy for seawater desalination, Chem. Eng. J. 166 (2011) 596-606.
6. A. Chafidz, E.D. Kerme, I. Wazeer, Y. Khalid, A. Ajbar, and S.M. Al-Zahrani, Design and fabrication of a portable and hybrid solar-powered membrane distillation system, J. Clean. Prod. 133 (2016) 631-647.
7. G. Naidu, S. Jeong, Y. Choi, E. Jang, T.-M. Hwang, and S. Vigneswaran, Application of vacuum membrane distillation for small scale drinking water production, Desalination 354 (2014) 53-61.
8. H. Chang, S.-G. Lyu, C.-M. Tsai, Y.-H. Chen, T.-W. Cheng, and Y.-H. Chou, Experimental and simulation study of a solar thermal driven membrane distillation desalination process, Desalination 286 (2012) 400-411.
9. J. Plattner, G. Naidu, T. Wintgens, S. Vigneswaran, and C. Kazner, Fluoride removal from groundwater using direct contact membrane distillation (DCMD) and vacuum enhanced DCMD (VEDCMD), Sep. Purif. Technol. 180 (2017) 125-132.
10. H.C. Duong, P. Cooper, B. Nelemans, T.Y. Cath, and L.D. Nghiem, Evaluating energy consumption of membrane distillation for seawater desalination using a pilot air gap system, Sep. Purif. Technol. 166 (2016) 55-62.

11. H.C. Duong, M. Duke, S. Gray, T.Y. Cath, and L.D. Nghiem, Scaling control during membrane distillation of coal seam gas reverse osmosis brine, J. Membr. Sci. 493 (2015) 673-682.

12. V.A. Ravisankar, R. Seaman, S. Mirchandani, R.G. Arnold, and W.P. Ela, Solar-driven membrane distillation demonstration in Leupp, Arizona, Rev. Environ. Health 31 (2016) 79-83.

13. A. Alkhudhiri, N. Darwish, and N. Hilal, Membrane distillation: A comprehensive review, Desalination 287 (2012) 2-18.

14. N. Dow, S. Gray, J.-d. Li, J. Zhang, E. Ostarcevic, A. Liubinas, P. Atherton, G. Roeszler, A. Gibbs, and M. Duke, Pilot trial of membrane distillation driven by low grade waste heat: Membrane fouling and energy assessment, Desalination 391 (2016) 30-42.

15. L.D. Nghiem, F. Hildinger, F.I. Hai, and T. Cath, Treatment of saline aqueous solutions using direct contact membrane distillation, Desalin. Water Treat. 32 (2011) 234-241.

16. F. Suárez, J.A. Ruskowitz, S.W. Tyler, and A.E. Childress, Renewable water: Direct contact membrane distillation coupled with solar ponds, Appl. Energy 158 (2015) 532-539.

17. W.G. Shim, K. He, S. Gray, and I.S. Moon, Solar energy assisted direct contact membrane distillation (DCMD) process for seawater desalination, Sep. Purif. Technol. 143 (2015) 94-104.

18. F. Banat, N. Jwaied, M. Rommel, J. Koschikowski, and M. Wieghaus, Desalination by a "compact SMADES" autonomous solar-powered membrane distillation unit, Desalination 217 (2007) 29-37.

19. H.E.S. Fath, S.M. Elsherbiny, A.A. Hassan, M. Rommel, M. Wieghaus, J. Koschikowski, and M. Vatansever, PV and thermally driven small-scale, stand-alone solar desalination systems with very low maintenance needs, Desalination 225 (2008) 58-69.

20. J. Koschikowski, M. Wieghaus, and M. Rommel, Solar thermal-driven desalination plants based on membrane distillation, Desalination 156 (2003) 295-304.

21. H. Yu, X. Yang, R. Wang, and A.G. Fane, Analysis of heat and mass transfer by CFD for performance enhancement in direct contact membrane distillation, J. Membr. Sci. 405-406 (2012) 38-47.

22. Y. Taamneh and K. Bataineh, Improving the performance of direct contact membrane distillation utilizing spacer-filled channel, Desalination 408 (2017) 25-35.

23. A.M. Karam, A.S. Alsaadi, N. Ghaffour, and T.M. Laleg-Kirati, Analysis of direct contact membrane distillation based on a lumped-parameter dynamic predictive model, Desalination 402 (2017) 50-61.

24. G. Dong, J.F. Kim, J.H. Kim, E. Drioli, and Y.M. Lee, Open-source predictive simulators for scale-up of direct contact membrane distillation modules for seawater desalination, Desalination 402 (2017) 72-87.

25. J. Deshpande, K. Nithyanandam, and R. Pitchumani, Analysis and design of direct contact membrane distillation, J. Membr. Sci. 523 (2017) 301-316.

26. M. Ghadiri, S. Fakhri, and S. Shirazian, Modeling of water transport through nanopores of membranes in direct-contact membrane distillation process, Polym. Eng. Sci. 54 (2014) 660-666.

27. Y.M. Manawi, M. Khraisheh, A.K. Fard, F. Benyahia, and S. Adham, Effect of operational parameters on distillate flux in direct contact membrane distillation (DCMD): Comparison between experimental and model predicted performance, Desalination 336 (2014) 110-120.

28. H. Chang, G.-B. Wang, Y.-H. Chen, C.-C. Li, and C.-L. Chang, Modeling and optimization of a solar driven membrane distillation desalination system, Renew. Energy 35 (2010) 2714-2722.

29. J.-G. Lee, W.-S. Kim, J.-S. Choi, N. Ghaffour, and Y.-D. Kim, Dynamic solar-powered multi-stage direct contact membrane distillation system: Concept design, modeling and simulation, Desalination (2017), http://dx.doi.org/10.1016/j.desal.2017.04.008.

30. R.G. Raluy, R. Schwantes, V.J. Subiela, B. Peñate, G. Melián, and J.R. Betancort, Operational experience of a solar membrane distillation demonstration plant in Pozo Izquierdo-Gran Canaria Island (Spain), Desalination 290 (2012) 1-13.

31. Solar Energy Laboratory, University of Wisconsin-Madison, TRNSYS 17: a Transient System Simulation Program, (2014).

32. M. Qtaishat, T. Matsuura, B. Kruczek, and M. Khayet, Heat and mass transfer analysis in direct contact membrane distillation, Desalination 219 (2008) 272-292.

33. J. Zhang, S. Gray, and J.-D. Li, Modelling heat and mass transfers in DCMD using compressible membranes, J. Membr. Sci. 387-388 (2012) 7-16.

34. J. Phattaranawik, R. Jiraratananon, and A.G. Fane, Heat transport and membrane distillation coefficients in direct contact membrane distillation, J. Membr. Sci. 212 (2003) 177-193.

35. M. Khayet, A. Velázquez, and J.I. Mengual, Modelling mass transport through a porous partition: Effect of pore size distribution, J. Non-Equilib. Thermodyn. 29 (2004) 279-299.

36. I. Hitsov, T. Maere, K. De Sitter, C. Dotremont, and I. Nopens, Modelling approaches in membrane distillation: A critical review, Sep. Purif. Technol. 142 (2015) 48-64.

37. M. Gryta, M. Tomaszewska, and A.W. Morawski, Membrane distillation with laminar flow, Sep. Purif. Technol. 11 (1997) 93-101.

38. I. Hitsov, L. Eykens, W.D. Schepper, K.D. Sitter, C. Dotremont, and I. Nopens, Full-scale direct contact membrane distillation (DCMD) model including membrane compaction effects, J. Membr. Sci. 524 (2017) 245-256.

39. A. Katsandri, A theoretical analysis of a spacer filled flat plate membrane distillation modules using CFD: Part II: Temperature polarisation analysis, Desalination 408 (2017) 166-180.

40. P. Termpiyakul, R. Jiraratananon, and S. Srisurichan, Heat and mass transfer characteristics of a direct contact membrane distillation process for desalination, Desalination 177 (2005) 133-141.

545 41. Y. Yun, J. Wang, R. Ma, and A.G. Fane, Effects of channel spacers on direct contact
546 membrane distillation, Desalin. Water Treat. 34 (2011) 63-69.

547 42. J. Phattaranawik, R. Jiraratananon, and A.G. Fane, Effects of net-type spacers on heat and
548 mass transfer in direct contact membrane distillation and comparison with ultrafiltration
549 studies, J. Membr. Sci. 217 (2003) 193-206.

550 43. J.-G. Lee, Y.-D. Kim, W.-S. Kim, L. Francis, G. Amy, and N. Ghaffour, Performance
551 modeling of direct contact membrane distillation (DCMD) seawater desalination process
552 using a commercial composite membrane, J. Membr. Sci. (2015).

553 44. H.C. Duong, F.I. Hai, A. Al-Jubainawi, Z. Ma, T. He, and L.D. Nghiem, Liquid desiccant
554 lithium chloride regeneration by membrane distillation for air conditioning, Sep. Purif.
555 Technol. 177 (2017) 121-128.

556 45. H.C. Duong, P. Cooper, B. Nelemans, T.Y. Cath, and L.D. Nghiem, Evaluating energy
557 consumption of air gap membrane distillation for seawater desalination at pilot scale
558 level, Sep. Purif. Technol. 166 (2016) 55-62.

559 46. H.C. Duong, P. Cooper, B. Nelemans, and L.D. Nghiem, Optimising thermal efficiency of
560 direct contact membrane distillation via brine recycling for small-scale seawater
561 desalination, Desalination 374 (2015) 1-9.

562 47. H.C. Duong, M. Duke, S. Gray, P. Cooper, and L.D. Nghiem, Membrane scaling and
563 prevention techniques during seawater desalination by air gap membrane distillation,
564 Desalination 397 (2016) 92-100.